



HAL
open science

Radiation-Induced Leakage Current and Electric Field Enhancement in CMOS Image Sensor Sense Node Floating Diffusions

Alexandre Le Roch, Cédric Virmontois, Philippe Paillet, Jean-Marc Belloir, Serena Rizzolo, Federico Pace, Clémentine Durnez, Pierre Magnan, Vincent Goiffon

► **To cite this version:**

Alexandre Le Roch, Cédric Virmontois, Philippe Paillet, Jean-Marc Belloir, Serena Rizzolo, et al.. Radiation-Induced Leakage Current and Electric Field Enhancement in CMOS Image Sensor Sense Node Floating Diffusions. *IEEE Transactions on Nuclear Science*, 2019, 66 (3), pp.616-624. 10.1109/TNS.2019.2892645 . hal-02103366

HAL Id: hal-02103366

<https://hal.science/hal-02103366>

Submitted on 18 Apr 2019

HAL is a multi-disciplinary open access archive for the deposit and dissemination of scientific research documents, whether they are published or not. The documents may come from teaching and research institutions in France or abroad, or from public or private research centers.

L'archive ouverte pluridisciplinaire **HAL**, est destinée au dépôt et à la diffusion de documents scientifiques de niveau recherche, publiés ou non, émanant des établissements d'enseignement et de recherche français ou étrangers, des laboratoires publics ou privés.



Open Archive Toulouse Archive Ouverte (OATAO)

OATAO is an open access repository that collects the work of some Toulouse researchers and makes it freely available over the web where possible.

This is an author's version published in: <https://oatao.univ-toulouse.fr/22965>

Official URL : <http://doi.org/10.1109/TNS.2019.2892645>

To cite this version :

Le Roch, Alexandre and Virmontois, Cédric and Paillet, Philippe and Belloir, Jean-Marc and Rizzolo, Serena and Pace, Federico and Durnez, Clémentine and Magnan, Pierre and Goiffon, Vincent Radiation-Induced Leakage Current and Electric Field Enhancement in CMOS Image Sensor Sense Node Floating Diffusions. (2019) IEEE Transactions on Nuclear Science, 66 (3). 616-624. ISSN 0018-9499

Any correspondence concerning this service should be sent to the repository administrator:

tech-oatao@listes-diff.inp-toulouse.fr

Radiation-Induced Leakage Current and Electric Field Enhancement in CMOS Image Sensor Sense Node Floating Diffusions

Alexandre Le Roch¹, Student Member, IEEE, Cédric Virmondois, Member, IEEE, Philippe Paillet², Member, IEEE, Jean-Marc Belloir², Serena Rizzolo³, Member, IEEE, Federico Pace, Student Member, IEEE, Clémentine Durnez⁴, Member, IEEE, Pierre Magnan, Member, IEEE, and Vincent Goiffon⁵, Member, IEEE

Abstract—This paper investigates the leakage currents as well as the leakage current Random Telegraph Signals (RTSs) sources in sense node floating diffusions (FDs) and their consequences on imaging performances specifically after exposure to high-energy particle radiation. Atomic displacement damage and ionization effects are separately studied thanks to neutron and X-ray irradiations. Proton irradiations have been performed to simultaneously study displacement damage dose (DDD) and total ionizing dose (TID) effects while being more representative of the space environment. The studied DDD ranges from $500 \text{ TeV} \cdot \text{g}^{-1}$ to $40 \text{ GeV} \cdot \text{g}^{-1}$, and the TID ranges from $24 \text{ krad}(\text{SiO}_2)$ to $72 \text{ krad}(\text{SiO}_2)$. High-magnitude electric field effects, such as transfer-gate-induced leakage current, are investigated to further understand the phenomena involved in FDs while giving new insights into the Electric Field Enhancement of the charge generation mechanisms. This paper shows that FDs are very sensitive to ionizing radiation because of the presence of depleted Si/SiO₂ interface with high-magnitude electric fields around the junction. On the other hand, displacement damage in the FDs is a major source of high amplitude leakage current RTSs and leakage current nonuniformity. Such radiation-induced degradations can prevent the use of CMOS image sensor with long FD retention time (e.g., global shutter operating mode or burst imagers) in radiation environments.

Index Terms—Charge storage, CMOS image sensor (CIS), dark current (DC), displacement damage dose (DDD), Electric Field Enhancement (EFE), floating diffusion (FD), global shutter, leakage current, pinned photodiode (PPD), Random Telegraph Signal (RTS), sense node (SN), total ionizing dose (TID).

I. INTRODUCTION

CMOS image sensors (CISs), also called active pixel sensors (APSSs), are solid-state imaging arrays where the transistors are integrated within the pixels. Among CISs, the four-transistor (4T) pinned photodiode (PPD) CIS, which

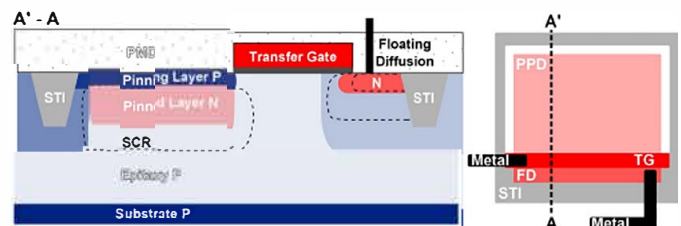


Fig. 1. Cross section and top view of a 4T PPD pixel.

cross section and top view are both shown in Fig. 1, is composed of pixels made of a buried photodiode (the PPD), a transfer gate (TG), a sense node (SN) floating diffusion (FD), and three other transistors, which are not represented, for reset and readout purposes [1]. Once the collected charges are transferred from the PPD to the FD throughout the TG by joining the two space-charged regions, they are stored for a certain amount of time, differing from the integration time, before being readout. For some specific applications using long-duration charge storage in FDs such as CISs operated in global shutter mode or burst mode, the role of the FDs becomes prominent [2], [3]. Indeed, contrary to the rolling shutter CISs, the long storage time in FDs required in global shutter image sensors makes them very sensitive to FD leakage current. Since global shutter and burst CISs are considered in various space and scientific applications in harsh radiation environments, it appears necessary to study radiation-induced FD leakage current in CISs.

Radiation-induced leakage currents in CISs photodiodes, also called dark current (DC), have been extensively studied both in the conventional photodiode and PPD technologies and reported therein [4]. Among these sources, two distinct phenomena can be differentiated: first, a continuous leakage current based on the Shockley–Read–Hall kinetic with a constant generation rate [5] and second, a leakage current fluctuation called Random Telegraph Signal (RTS) characterized by a random and discrete fluctuations of the leakage current presenting several generation rates [6]–[8]. The origin of these fluctuations remains unclear but possibly relies on metastable generation centers presenting several configurations leading to several generation rates [6], [9]. Due to its random

¹A. Le Roch, S. Rizzolo, F. Pace, C. Durnez, P. Magnan, and V. Goiffon are with ISAE-SUPAERO, Université de Toulouse, F-31055 Toulouse, France (e-mail: alexandre.le-roch@isae-supero.fr).

²C. Virmondois and J.-M. Belloir are with the Center National d'Etudes Spatiales, F-31400 Toulouse, France.

³P. Paillet is with CEA, DAM, DIF, F-91297 Arpajon, France.

fluctuations as well as its high leakage current variations, this parasitic process severely affects the performances of CISs. Even though numerous studies focus on leakage current sources in CISs photodiodes, a very few works are dedicated to the FD leakage current [10], and none is dedicated to the radiation effects on the FD leakage current.

II. EXPERIMENTAL DETAILS

This section aims to describe the sensors under test as well as the setup used to characterize the leakage current and the leakage current RTS before and after irradiation. The CIS under test is a 512×512 4T PPD custom imager manufactured in a commercially available 180-nm CIS technology. This sensor has been designed and built for scientific research purposes allowing modifying most of the relevant potentials in the pixels. The structure of the pixels is similar to the illustration presented in Fig. 1. As this paper focuses on the FD structure, the CIS is operated as 3T CISs where the FD is assimilated to the photosensitive element. To do so, the TG is kept at its low bias level (OFF condition), and variable FD integration time is inserted between the signal and the reference samples. This FD integration time is directly linked to the retention time in the case of a global shutter configuration as well as in the case of any application where the signal is stored in-pixel on an FD. All the measurements are performed in the dark at 22 °C. Leakage current RTS analysis uses a rising edge detection algorithm [11], [12] with a 1-s sampling period on 15 000 images. The considered neutron and proton irradiations were performed at Université Catholique de Louvain in Louvain, Belgium. X-ray irradiation was performed using an Aracor 10 keV X-ray irradiator at CEA DAM in Bruyère le Chatel, France. Irradiation parameters are summarized in Table I and were performed at room temperature with all the CIS pins grounded.

In this paper, the influence of the electric field on the FD leakage current is investigated using the TG low bias level (i.e., the TG OFF-voltage) from 0 to -1 V and the reset supply voltage from 1.8 to 3.3 V. The nominal bias conditions for Sections III and IV are 0 V for the TG and 3.3 V for the reset voltage. All the measurements have been performed after four weeks of annealing at room temperature. In order to compare the results obtained on the FD to the PPD technology addressed in many papers, this paper investigates both the PPD and the FD leakage current sources on the same sensor.

III. RADIATION EFFECTS ON THE LEAKAGE CURRENT

This section first addresses the radiation-induced mean leakage current increase over the sensor array. Results are compared with the universal damage factor (UDF) [13]. Then, the leakage current distribution is investigated giving more insights into the leakage current nonuniformity induced by radiation.

A. Mean Leakage Current

The mapping of PPD and FD leakage current over a small part of the sensor arrays is shown in Fig. 2. Before irradiation, while the mean leakage current in PPDs is only about $8 \text{ e}^- \cdot \text{s}^{-1}$

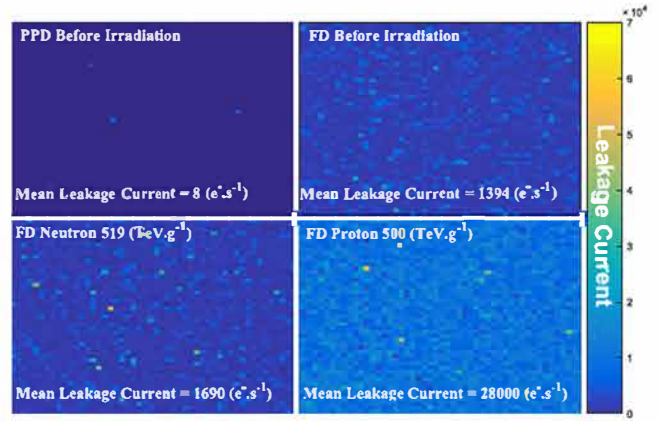


Fig. 2. Image depicting the leakage current in the PPDs before irradiation and in the FDs before and after irradiation.

at 22 °C, the mean leakage current in FDs is about $1400 \text{ e}^- \cdot \text{s}^{-1}$ at the same temperature. In the absence of radiation-induced degradation, the PPD depletion region does not reach any oxide. Hence, only silicon bulk defects could possibly bring a generation current contribution. Since the PPD exhibits a very low mean leakage current before irradiation, we can legitimately suppose that the PPD is almost free of bulk defect. This conclusion can be transposed to the FD, which shares the same silicon bulk. Hence, it can be inferred that the FD leakage current comes from generation centers located at the Si/SiO₂ interface, such as the TG oxide and the shallow trench isolation (STI) sidewalls, which are directly in contact with the FD depleted regions, as shown in Fig. 1. Such interface defects are known to be leakage current sources and are generally reduced by a process in the conventional photodiodes [1]. SN FDs usually do not benefit from such manufacturing process optimization, and it does not appear surprising to measure such an intense leakage current before irradiation. Moreover, the FD mean leakage current is even more important after irradiation. Similar displacement damage dose (DDD) induced by neutron and proton irradiations has been deposited in sensors and labeled as A/B and E/F , respectively, in Table I. The mean leakage current after proton irradiation is one order of magnitude higher than the one after neutron irradiation as shown in Fig. 2 for $\text{DDD} = 500 \text{ TeV} \cdot \text{g}^{-1}$. This result points out the high sensitivity of the FDs leakage current to the total ionizing dose (TID). In FDs, the leakage current is dominated by Si/SiO₂ interface defects before irradiation and by TID-induced interface defects after ionizing energy exposition.

The mean leakage current increase per unit volume measured all over the sensor array after irradiations are reported in Fig. 3 both for PPDs and FDs. Focusing on the PPDs results, we observe an increase of the mean leakage current for all the irradiations. The considered PPD depleted volume is $23 \mu\text{m}^3$. The UDF model [13], which includes exclusively the displacement damage contribution, is in agreement with the experimental mean leakage current increase in PPD for both neutron and proton irradiations. These results confirm that the TID-induced leakage current in PPDs is negligible in front of the displacement damage contribution for 50-MeV protons on the considered TID range.

TABLE I
IRRADIATION PARAMETERS

Sensor Ref	A	B	C	D	E	F	G
Particle	Neutron	Neutron	Neutron	Neutron	Proton	Proton	X-Ray
Energy (MeV)	22	22	22	22	49.7	49.7	10×10^{-3}
Fluence (cm^{-2})	1.3×10^{11}	3.9×10^{11}	1.0×10^{12}	1.0×10^{13}	1.3×10^{11}	3.8×10^{11}	-
NIEL ($\text{keV} \cdot \text{cm}^{-2} \cdot \text{g}^{-1}$)	3.99	3.99	3.99	3.99	3.97	3.97	-
DDD ($\text{TeV} \cdot \text{g}^{-1}$)	519	1560	4000	40000	500	1500	-
1 MeV Neutron Fluence (cm^{-2})	2.71×10^{11}	8.13×10^{11}	2.09×10^{12}	2.71×10^{13}	2.61×10^{11}	7.82×10^{11}	-
LET ($\text{MeV} \cdot \text{cm}^{-2} \cdot \text{g}^{-1}$)	-	-	-	-	11.9	11.9	-
TID (krad(SiO_2))	-	-	-	-	24.1	72.2	24.0

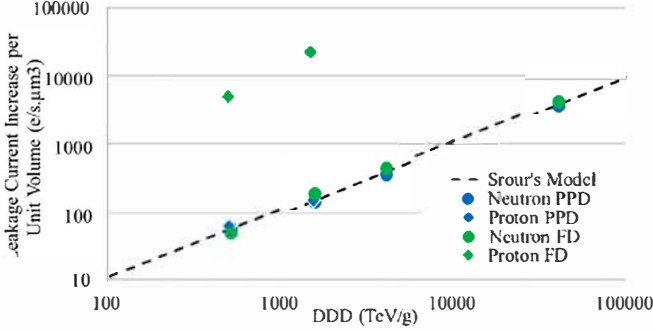


Fig. 3. Evolution of the mean leakage current increase per unit volume with irradiations. The considered UDF value after one month annealing is $K_{\text{dark}} = 0.098 \text{ e}^- \cdot \text{s}^{-1} / \text{TeV} \cdot \text{g}^{-1} / \mu\text{m}^3$ [13].

Regarding the FDs mean leakage current increase after neutron irradiations, these results are also in good agreement with the UDF considering an FD depleted region of $6 \mu\text{m}^3$. Since the UDF model is clearly applicable after neutron irradiations in the FD, it implies that the majority of defects, which have been created into the studied depleted volume, are not impacted by a significant Electric Field Enhancement (EFE). Indeed, it would have led to a mean leakage current increase higher than the UDF model prediction.

After proton irradiations, the FD mean leakage current increase does not fit the UDF model prediction as shown in Fig. 3. This can be explained by the ionizing energy deposited by the protons leading to a multitude of Si/SiO₂ interface defects as observed in conventional photodiodes without surface pinning implant (i.e., the so-called 3T photodiodes) [4].

B. Leakage Current Distribution

The PPD leakage current (i.e. DC) distributions before and after irradiations are shown in Fig. 4. All the irradiations lead to a commonly observed leakage current tail, which increases with the deposited DDD. The similar distributions observed after neutron and proton irradiations, which have induced the same DDD, confirm that, on the whole PPD population, TID effects are negligible in front of DDD effects for 50-MeV protons on the considered TID (24 krad). The PPD leakage current distributions induced by DDD have been studied in numerous papers, and several empirical models have already been proposed [14]–[16]. Simulation-based models have also been presented in the literature [17]. In this paper,

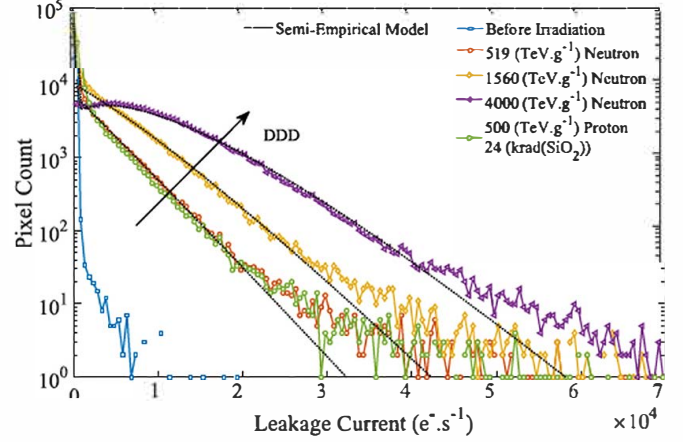


Fig. 4. Distributions of the PPDs leakage current after 50-MeV protons and 22-MeV neutrons irradiations.

the analytical model developed in [18] is considered because it does not require any simulation and has been verified on several CIS technologies. The leakage current of one pixel after irradiation I_{darkDDD} can be expressed as

$$I_{\text{darkDDD}} = I_{\text{dark}} + \Delta I_{\text{darkDDD}} \quad (1)$$

where I_{dark} is the leakage current before irradiation and $\Delta I_{\text{darkDDD}}$ is the DDD-induced leakage current increase. Using the probability density function (pdf) to study the whole population of pixel over this array, the expression (1) becomes

$$f_{\text{darkDDD}}(x) = f_{\text{dark}}(x) * f_{\Delta I_{\text{darkDDD}}}(x) \quad (2)$$

where $f_{\Delta I_{\text{darkDDD}}}(x)$ is detailed in the Appendix. As expected, the leakage current increase distributions after irradiations are in good agreement with this DDD semiempirical model, demonstrating once again that bulk defects dominate the PPD response in these irradiation conditions. The good agreement with the model also demonstrates clearly that EFE does not play a significant role on irradiated PPDs since EFE is not taken into account in the model.

Fig. 5 shows the FDs leakage current distributions before and after irradiations. Before irradiation, the FDs leakage current distribution discloses a large leakage current tail in comparison with the one observed in PPDs visible in Fig. 4. Moreover, this distribution looks bent. This observation does not correspond to the leakage current distributions of the conventional 3T photodiodes dominated by Si/SiO₂ interface defects [19]. These results could be explained by an EFE of the FDs leakage current of some pixels as discussed in [20]

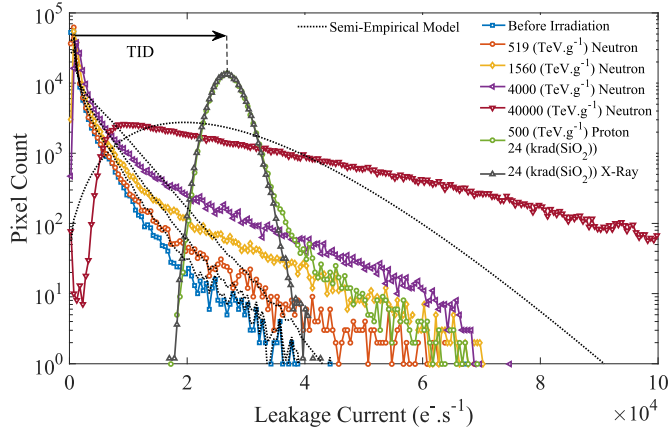


Fig. 5. Distributions of the FDs leakage current after 50-MeV protons and 22-MeV neutrons irradiations.

and [21]. Hence, these observations suggest that FDs have intrinsic high-magnitude electric field regions, which could influence the FDs leakage current distribution.

After neutron irradiations, the rise of the FDs leakage current tail with the deposited DDD is observed. However, the semiempirical model used to predict the leakage current distribution after neutron irradiation does not fit the experimental results gathered on the FDs, as shown in Fig. 5. Indeed, it appears a leakage current distribution tail extension toward higher leakage current compensated by a reduction of the occurrence at lower leakage current values. It leads to a bend of the leakage current distribution tail, which is more and more obvious with increasing deposited DDD. This discrepancy from the model suggests that the DDD-induced defects behave differently in the FDs. The previously suggested presence of high electric field regions in the FDs before irradiation could also explain this observation by enhancing the carrier generation rates of the bulk defects induced by the DDD. This EFE is not visible on the average leakage current value (see Section III-A) because only a small population of pixels is dominated by this effect.

Contrary to what is seen on PPDs (see Fig. 4), the TID contribution induced either by proton or X-ray irradiations in the FD leakage current is visible in Fig. 5 as a clear Gaussian distribution centered on $2.8 \times 10^4 \text{ e}^- \cdot \text{s}^{-1}$. The fact that the TID increases the FD leakage current of the whole pixel population is also clearly visible in Fig. 3 when comparing proton to neutron irradiations. Hence, it can be concluded that, after ionizing dose deposition, the FDs leakage current is mainly due to the creation of additional interface defects located either at the STI sidewalls or under the TG gate oxide.

Regarding the comparison between protons and X-rays, both irradiations share the same TID and reveal the same mean leakage current as well as the same Gaussian distribution as expected. Although after proton irradiation the mean leakage current is dominated by the interface state contribution, the distribution still reveals a leakage current tail, which corresponds to the DDD induced leakage current nonuniformity.

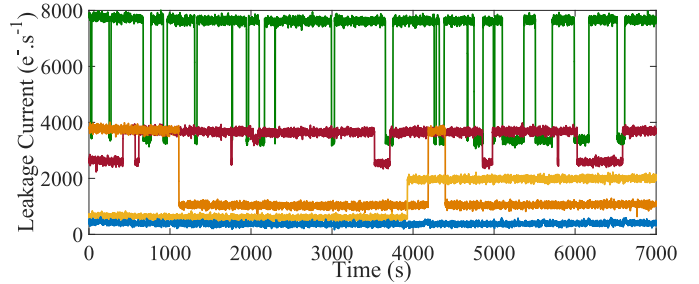


Fig. 6. Leakage current evolution with time of five FDs before irradiation. Four of them are exhibiting a leakage current RTS behavior.

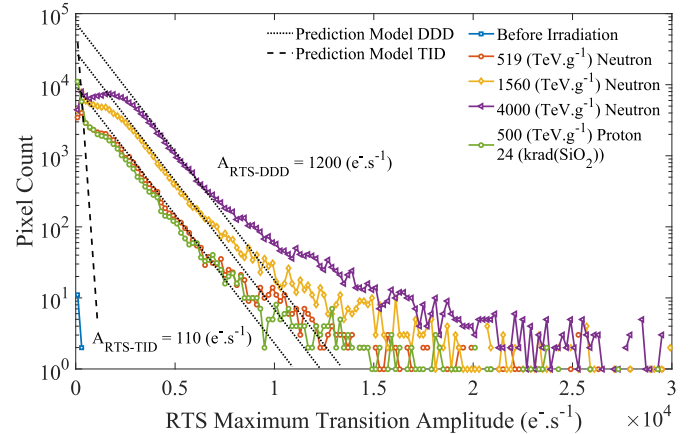


Fig. 7. Distributions of the PPDs RTS maximum transition amplitude of the leakage current before and after 50-MeV protons and 22-MeV neutrons irradiations.

IV. RADIATION EFFECTS ON THE LEAKAGE CURRENT RANDOM TELEGRAPH SIGNAL

Fig. 6 shows the FD leakage current RTS evolution with time of five selected pixels of an unirradiated sensor. Fig. 6 shows that the FDs are already exhibiting the clear leakage current RTS behaviors before irradiation as reported in [10]. Over the sensor array, 5% of the FDs disclose the RTS behavior versus 0.04% for the PPDs.

The leakage current RTS maximum transition amplitude distributions before and after irradiation are presented in Fig. 7 for the PPDs. The prediction model proposed in [4] and [11] is in good agreement with the experimental data after DDD deposition by 22-MeV neutrons and 50-MeV protons. The typical mean RTS maximum transition amplitude is at $A_{\text{rts}} = 1200 \text{ e}^- \cdot \text{s}^{-1}$ as expected at room temperature. For high DDD deposition, the prediction model underestimates the end of the RTS maximum transition amplitude distribution tail. This could be due to the presence of the second RTS center population with a higher amplitude than the main one, also observed in [22], which would only be visible when the studies RTS center population is large enough. The study of this deviation will be the subject of future work. The proton irradiation generates a clear peak at low RTS amplitude that corresponds to the TID contribution with a typical mean RTS maximum transition amplitude of $A_{\text{rts}} = 110 \text{ e}^- \cdot \text{s}^{-1}$ at room temperature as reported in [23]. The main conclusion here is that the main RTS center population in the PPD is

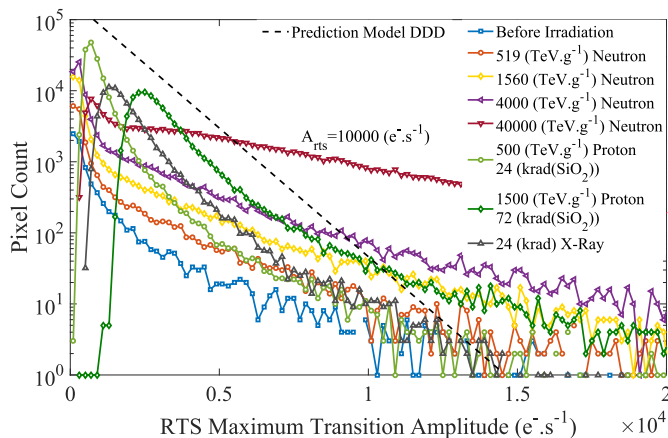


Fig. 8. Distributions of the FDs RTS maximum transition amplitude of the leakage current before and after 50-MeV protons and 22-MeV neutrons irradiations. The slope of the prediction model is at $A_{rts} = 1200 e^- \cdot s^{-1}$.

well described by the existing predicting model for 22-MeV neutron and 50-MeV proton irradiations in the studied CMOS technology.

The leakage current RTS maximum transition amplitude distributions before and after irradiations are presented in Fig. 8 for the FDs. Unlike the PPDs which can be impacted by a low level of DDD as shown in Fig. 7, the relative increase in the RTS behavior at low DDD is less obvious in FDs, as shown in Fig. 8. Indeed, in the FD, the leakage current RTS is dominated by preirradiation interface defects as mentioned for the average leakage current. Once the sufficient DDD to obtain a clear signature of the DDD-induced RTS center is reached, an unusual RTS maximum transition amplitude distribution with a mean value of $A_{rts} = 10000 e^- \cdot s^{-1}$ appears. This value is one order of magnitude higher than the classical value validated on many CMOS and CCD sensors ($A_{rts} = 1200 e^- \cdot s^{-1}$) and reported in [19]. This discrepancy could be due to a high-magnitude electric field effect, which would enhance the RTS defects generation rates. This hypothesis may seem to contradict the conclusion made in Section III-A, stating that the radiation-induced mean leakage current increase in the FDs is not enhanced by the electric field. However, the used RTS detection method detects the response of a single RTS center per pixel, the one that exhibits the largest maximum transition amplitude. Hence, this technique isolates and highlights the most intense RTS fluctuations and hides the weakest ones, whereas the mean leakage current analysis averages the response of all the defects in a pixel, hiding the possible EFE. Therefore, it can be inferred that the high-magnitude electric field regions do not influence significantly the average leakage current increase in the FDs, but EFE plays a major role in the most extreme behaviors (i.e., the leakage current distribution tail and the leakage current RTS amplitudes).

After ionizing dose deposition either induced by X-rays or protons, the FD RTS maximum transition amplitude distributions do not follow the classical trend observed in the conventional photodiodes and PPDs. Indeed, the typical exponential distribution coming from the Si/SiO₂ interface defects usually induced by the TID with an RTS maximum transition amplitude of $A_{rts} = 110 e^- \cdot s^{-1}$ [24] is not observed. Instead,

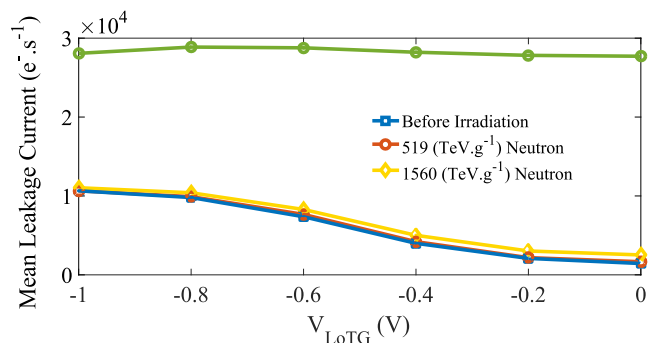


Fig. 9. Evolution of the FD leakage current with TG OFF-voltage before and after 50-MeV protons and 22-MeV neutrons irradiations.

the FDs reveal an unusual bent distribution, which could be explained here again by the presence of high-magnitude electric field regions, but this time at the Si/SiO₂ interface since they influence directly the TID-induced interface defect generation rates. The enhancement of TID-induced oxide RTS seems important enough to hide the DDD-induced RTS in the case of 50-MeV proton irradiations.

V. INDUCED ELECTRIC FIELD EFFECTS ON THE FD LEAKAGE CURRENT

After having suggested the existence of high-magnitude intrinsic electric field regions in the FD leading to an EFE of the defects generation rates, this section aims to highlight the role of this electric field by varying the biasing conditions.

A. Effects of the Transfer-Gate Bias on Leakage Currents

The structure of a typical 4T PPD pixel is shown in Fig. 1. The role of the TG is to transfer the collected charges from the PPD to the FD by creating a conductive channel under the gate. To initiate the charge transfer, the TG is positively biased. However, during the integration time, the TG is negatively biased and isolates the photosensitive part, the PPD, from the FD SN. This last negative bias is commonly named V_{LoTG} and can be typically set in a product to a value between 0.5 and -1 V in an application to favor, respectively, an antiblooming behavior or a low PPD leakage current. In this experiment, the TG bias is kept at its low-level V_{LoTG} to study the FDs leakage current contribution and varies from 0 to -1 V.

Fig. 9 shows the FD mean leakage current versus the applied TG potential before and after irradiations. Before irradiation, the FD mean leakage current increases as the TG bias becomes more negative. The origin of this additional leakage current contribution in accumulation mode is similar to the one observed in MOSFET drains and 3T APS photodiodes in [25], which is referred to as gate-induced leakage trap-assisted tunneling (GIL-TAT) in [26] or more commonly as gate-induced drain leakage current [27], [28]. The location of this contribution is shown in Fig. 10 presenting the different leakage current sources in the FD structure. In the rolling shutter mode, the time delay between the reset sample and the signal sample is generally short enough (a few microseconds) to hide the effect of the FD GIL-TAT on the output signal. However, for longer FD charge storage durations, the FD

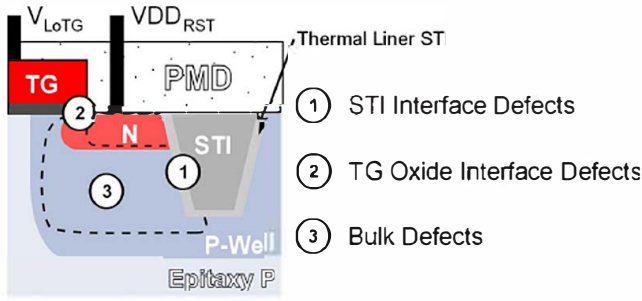


Fig. 10. Cross section of the FD structure showing the different leakage current sources.

GIL-TAT could be an important limitation parameter, and the high-negative TG bias should be avoided.

As shown in Fig. 9, neutron irradiations lead to a small increase of the FD mean leakage current. As the TG bias becomes more negative, the GIL-TAT is still observed but shifted upward because of the additional contribution of the neutron-induced leakage current. Radiation-induced bulk defects have no impact on the FDs mean leakage current in terms of GIL-TAT induced by the TG.

Contrary to the considered neutron irradiations in Fig. 9, the TID induced by the proton irradiation leads to a huge increase of the leakage current, which completely hides the GIL-TAT behavior on the average value. This result can be explained by the fact that the mean leakage current is mainly given by a large number of generated interface states that are not located in the GIL-TAT region 2 shown in Fig. 10.

The evolution of the FDs leakage current distribution before and after proton irradiation with the induced electric field is shown in Fig. 11. The previously observed GIL-TAT induced by the TG bias is visible before and after irradiation. Before irradiation, it results in a shift of the whole FDs leakage current distribution toward higher leakage currents. After the proton irradiation, it has been demonstrated in Section III-B that the distribution can be decomposed in two parts: a Gaussian part due to the TID induced interface states and a high leakage current distribution tail generated by the DDD-induced bulk defects. The negative bias of the TG only leads to a slight change of the Gaussian part of the leakage current distribution with no effect on the DDD-induced tail mentioned in Fig. 5. It clearly shows that GIL-TAT after the proton irradiation only has an influence on some rare oxide defects, probably located under the gate oxide, but that bulk defects are not influenced by the TG bias.

B. Effects of the Reset Voltage on Leakage Currents

During the reset phase of an operating 4T PPD CIS shown in Fig. 1, the reset transistor is turned on, and the FD is positively biased at the commonly named V_{DD_RST} potential. Once the FD capacity is charged, the reset transistor is turned off, and the charges coming from the leakage current sources are collected lowering the FD potential. As the generation rates of the FD leakage current sources can be impacted by the local electric field, FDs leakage current variation with the reset potential can be observed.

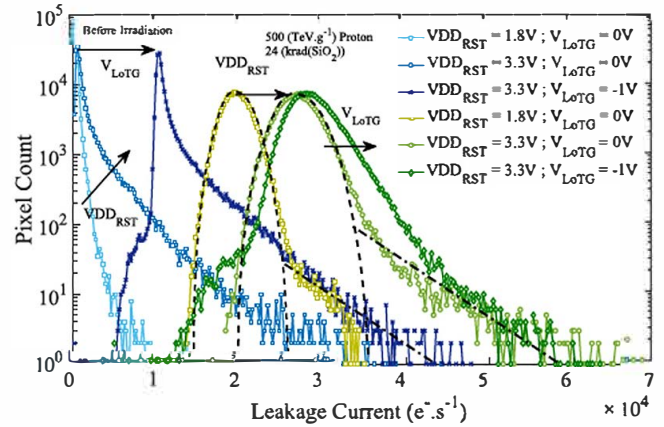


Fig. 11. FD leakage current distributions for several biasing conditions before and after proton irradiation $DDD = 500 \text{ TeV} \cdot \text{g}^{-1}$ and $TID = 24 \text{ krad}(\text{SiO}_2)$.

In addition to the effect of the TG bias, Fig. 11 shows the evolution of the FD leakage current distribution with the reset voltage-induced electric field before and after proton irradiation. Before irradiation, the reset voltage modulates directly the whole tail of the leakage current distribution, suggesting that this tail of high leakage currents is due to the defects located in a high-magnitude field region created by the reset voltage. Since the presence of bulk defects before irradiation is very unlikely, these defects at the origin of the distribution tails are probably oxide defects. It is clear in Fig. 11 that the TG voltage has no influence on the end of the leakage current tail. Hence, the defects responsible for the leakage current tail are not likely to be located in region 2 in Fig. 10. The most probable location of the leakage current tail defects before irradiation is the STI sidewalls including the corners and the photodiode angles (source 1 in Fig. 10). Their generation rates are probably enhanced by a local high-magnitude electric field (most likely in the corner vicinity) induced by the reset voltage.

After the proton irradiation, the impact of the reset voltage on the leakage current distribution is also visible in Fig. 11. As the reset voltage decreases, the leakage current distribution shifts toward low leakage current. This result can be explained by a reduction of the FD depleted volume lowering the number of active defects. On the other hand, it can also be caused by the reduction of the GIL-TAT contribution, which magnitude is related to the potential difference between the TG and the FD implant. By lowering the reset voltage from 3.3 to 1.8 V, the GIL-TAT is also reduced. Furthermore, this trend is also observed in Fig. 11 after the proton irradiation with the variation of the TG bias but at a lesser extent. The above-mentioned increase of the leakage current distribution tail with the reset voltage before irradiation is also visible after the proton irradiation in Fig. 11. The increase of the reset voltage results in a slight extension of the Gaussian distribution attributed to the TID contribution. As shown for the preirradiation interface states, the reset voltage has an impact on the TID-induced interface defects and probably enhances their generation rates. Regarding the leakage current tail attributed to the DDD induced by the proton irradiation,

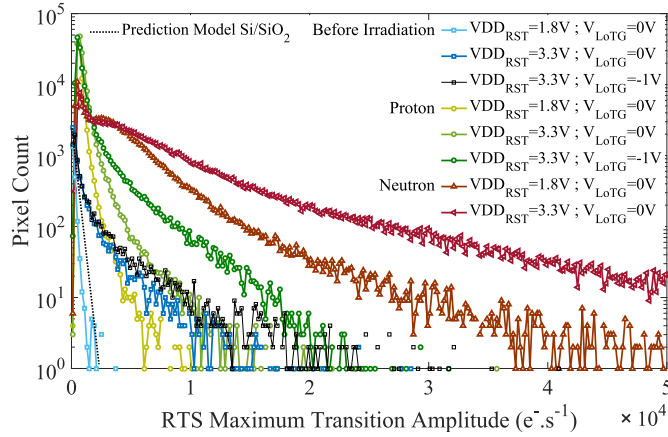


Fig. 12. FD leakage current RTS maximum transition amplitude distributions for several biasing conditions before and after neutron [DDD = 40 000 TeV · g⁻¹] and proton [DDD = 500 TeV · g⁻¹ and TID = 24 krad(SiO₂)] irradiations.

a reduction is observed with a decrease in the reset voltage, as shown in Fig. 11. Hence, these results suggest that the reset voltage has also an impact on the DDD-induced bulk defects generation rates.

To summarize, before irradiation, the reset voltage has an impact on the preirradiation defects located at the STI sidewalls including the corners and the photodiode angles. After irradiation, the reset voltage variation impacts both the TID- and DDD-induced defects.

C. Effects of the Transfer-Gate Bias on Leakage Current Random Telegraph Signals

As performed for the FD leakage current, this section focuses on the impacts of the induced electric field on the FDs leakage current RTS maximum transition amplitude. Fig. 12 shows the evolution of the FDs leakage current RTS maximum transition amplitude distribution with the induced electric field before irradiation (blue curves), after proton irradiation (green curves), and neutron irradiation (red curves). Before irradiation, the TG bias voltage does not influence the FDs leakage current RTS maximum transition amplitude distribution, showing that GIL-TAT does not play any role on the preirradiation RTS defects. The same results were observed after neutron irradiation. For the sake of clarity, the results are not reported in Fig. 12. As neutron irradiation does not lead to TID-induced defects, no high amplitude RTS contribution was observed with the TG bias variation.

After proton irradiation, biasing the TG more negatively leads to a clear EFE of the RTS maximum transition amplitudes, which extends the distribution toward higher RTS amplitudes. This high RTS amplitude contribution can be attributed to the TID-induced RTS defects located under the TG oxide, which are enhanced by the TG bias. This population can be linked to the one leading to the Gaussian deformation with the TG bias attributed to the TID-induced defect observed in Fig. 11. These results suggest that RTS defects located under the TG oxide do not play a major role in terms of leakage current RTS before irradiation but must be considered

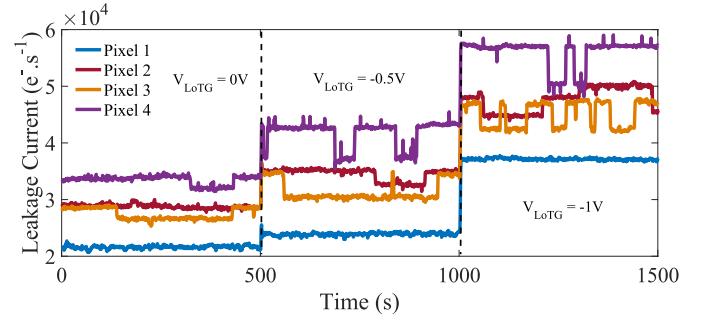


Fig. 13. FD leakage current evolution with the TG bias after proton irradiation 500 TeV · g⁻¹ and 24 krad(SiO₂).

after ionizing dose deposition as highlighted by the results shown in [29].

To illustrate these conclusions, the leakage current RTS evolution with time was followed while varying the bias applied on the TG. The results after the proton irradiation are presented in Fig. 13 for four selected pixels. The TG bias induces a classical GIL-TAT leakage current on pixel 1 by adding a continuous leakage current contribution, as shown in Fig. 11. For pixel 2, the GIL-TAT reveals a leakage current RTS behavior. Then, for pixels 3 and 4, the GIL-TAT clearly enhances the RTS amplitudes as already pointed out in Fig. 12.

D. Effects of the Reset Voltage on Leakage Current Random Telegraph Signals

In addition to the TG-induced effects, Fig. 12 shows the effects of the reset voltage on the RTS maximum transition amplitude distribution before and after proton and neutron irradiations. Before irradiation, the evolution of the RTS distribution with the reset voltage is clearly visible in Fig. 12. As the reset voltage decreases, the RTS distribution tail decreases and reveals an RTS maximum transition amplitude distribution slope at $A_{rts} = 110 \text{ e}^- \cdot \text{s}^{-1}$, which corresponds to the typical oxide DC-RTS signature in the absence of EFE.

After the proton irradiation, the increase of the reset voltage results in an extension of the RTS maximum transition amplitude distribution tail with no change in the main peak. As the RTS maximum transition amplitude distribution is dominated by interface states after ionizing energy deposition, it empathizes that the reset voltage plays a role on a small population of FDs presenting interface states with the leakage current RTS behavior.

Neutron irradiation sharing the same DDD than the studied proton irradiation leads to the same results as the one observed before irradiation because of the predominance of the preirradiation interface states in terms of leakage current RTS. After neutron-induced displacement at DDD = 40 000 TeV · g⁻¹, the reset voltage increase tends to increase the RTS maximum transition amplitude distribution tail. As the leakage current RTS is dominated by the induced DDD contribution at this dose, this result suggests that the reset voltage induced electric field plays a role on bulk RTS defects in the FD. Such reset voltage impact on the RTS behavior has not been observed in the 3T CIS photodiode [11]. This difference can be explained

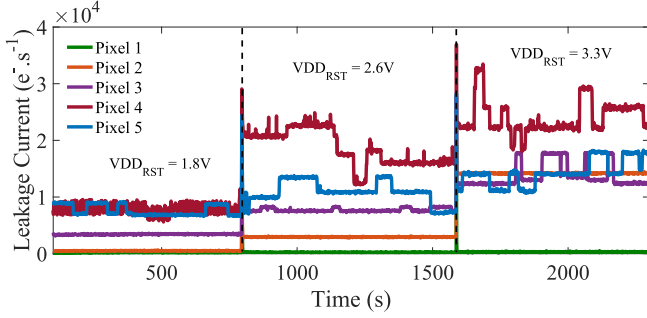


Fig. 14. FD leakage current evolution with the reset voltage after proton irradiation $500 \text{ TeV} \cdot \text{g}^{-1}$ and $24 \text{ krad}(\text{SiO}_2)$.

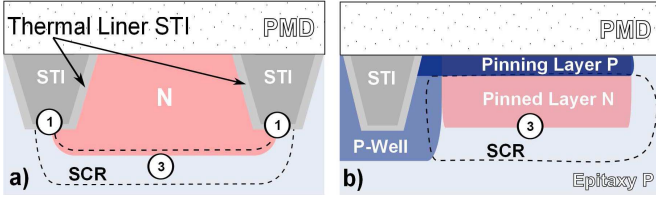


Fig. 15. Cross sections showing the different leakage current sources in the CIS photodiodes (to be compared with Fig. 10): ① STI interface defects and ③ DDD-induced bulk defects. (a) Conventional 3T photodiode found in 3T CISs. (b) PPD found in 4T-PPD CISs.

by the higher electric field involved in FDs in comparison with the 3T CIS photodiodes.

As for the influence of the TG biasing conditions, Fig. 14 shows the leakage current RTS evolution after the proton irradiation while varying the reset voltage on five selected pixels. As pixel 1, some of the FDs are not impacted at all by the reset voltage. On the contrary, pixel 2 has a leakage current, which generation rate is clearly enhanced with the reset voltage. Pixel 3 is an example of the pixel where the RTS behavior is revealed by the reset voltage. Finally, the pixels 4 and 5 exhibit the RTS amplitudes that are directly enhanced by the reset voltage induced electric field.

VI. CONCLUSION

Unlike for PPDs, the FD leakage current is dominated by the interface states contribution. Such defects are present before irradiation and are the limiting factor to reduce both the continuous leakage current and the leakage current RTS. Due to its high sensitivity to interface state density, the induced TID dominates the FDs leakage current contribution and is visible at low dose.

This paper also shows the behavior of the TID- and DDD-induced defects in the presence of high-magnitude electric field, which would explain the unusual leakage current and leakage current RTS distributions compared with the ones usually found in the optimized CIS photodiodes. Therefore, the results confirm that the EFE is not playing a significant role in the state-of-the-art CIS photodiodes. The field-assisted generation mechanisms identified in FDs are probably induced by the following three main characteristics shown in Fig. 10.

- 1) A high doping level of the n-implant into a p-well implant leading to a high-magnitude electric field within the p-n junction. Indeed, whereas the doping level of CIS photodiodes is optimized to avoid unwanted

high-magnitude electric field, the FD structure is based on a transistor source/drain implant with a higher doping level at the junction (e.g., $N_{\text{DFD}} \approx 10^{17} \text{ cm}^{-3}$ and $N_{\text{D3T-PD/PDD}} \approx 10^{15} \text{ cm}^{-3}$).

- 2) A large surface contact between the depleted region and the sidewalls of the STI. As shown in Fig. 15(a), depicting the cross section of a conventional 3T photodiodes, the doping profile of the n-implant is optimized to extend the depleted region at the bottom of the STIs avoiding the STI sidewalls and its corners. On the other hand, the PPD depleted region visible in Fig. 15(b) is totally isolated from the Si/SiO₂ interface. However, as shown in Fig. 10, the FD presents a large surface contact between its depleted volume and the STI sidewalls and thus all around the implant.
- 3) The proximity of the depleted region with the STI corners that present a high-magnitude electric field. Indeed, the FD depleted region can reach a few hundred of nanometers as shown in Fig. 10, leading to a contact with the corners of the STI generally presenting a high-magnitude electric field.

High-magnitude electric field effects induced both by the TG and the reset voltage have been investigated. It confirms the existence of an EFE in the FDs. The TG induces a GIL-TAT current based on the interface defects located at the oxide of the TG. This identified field-assisted leakage current is more important after the absorption of ionizing energy and can also lead to a leakage current RTS in this region. Therefore, the FD GIL-TAT will be considered when operating CIS requiring long retention time in radiation environments. The reset voltage also plays a prominent role in the electric field of the FDs and impacts the defects generation rates within the depleted region of the FD. The influence of the electric field on the defects generation rates is also relevant for other technologies, such as single photon avalanche diodes, which intentionally use a high-magnitude electric field to reach the breakdown voltage of the junction. Leakage current RTS investigation in such structures will certainly bring new experimental insights into the mechanisms involved in the field-assisted charge generation.

To improve the radiation resistance of FDs while allowing long storage times for global shutter CISs or burst CISs, the conventional hardening techniques of PN junctions can be considered. FD closed gate as used in [30] or charge storage in buried channels usually used for CCDs will be considered.

APPENDIX

DETAILS OF THE SEMIEMPIRICAL MODEL USED FOR THE LEAKAGE CURRENT DISTRIBUTION

The pdf of the DDD-induced leakage current increase $f_{\Delta I_{\text{darkDDDD}}}$, as introduced in [18], is based on an exponential pdf law to represent the leakage current increase contribution of a single nuclear interaction labeled $f_{\nu_{\text{dark}}}(x)$. This exponential law is expressed as

$$f_{\nu_{\text{dark}}}(x) = \frac{1}{\nu_{\text{dark}}} \exp\left(-\frac{x}{\nu_{\text{dark}}}\right). \quad (3)$$

The term ν_{dark} is the exponential mean of the pdf referring to the mean leakage current increase per nuclear interaction. It has been shown in [18] that $\nu_{\text{dark}} = 4100 \text{ e}^- \cdot \text{s}^{-1}$. At high DDD, the pdf is convoluted to account for the superimposition of nuclear interaction in the pixels. The total leakage current increase distribution $f_{\Delta I_{\text{darkDDD}}}(x)$ can be written as

$$f_{\Delta I_{\text{darkDDD}}}(x) = P(0, \mu) \times \delta(x) + P(1, \mu) \times f_{\nu_{\text{dark}}}(x) + P(2, \mu) \times f_{\nu_{\text{dark}}}(x) * f_{\nu_{\text{dark}}}(x) \dots \quad (4)$$

where P is the Poisson probability and μ is the mean number of nuclear interaction per pixel. In (4), the first term $P(0, \mu) \times \delta(x)$ accounting for nonimpacted pixels have been added to the expression introduced in [18]. It permits to conserve the integrity of the consider pixel population over the array. Thanks to this adaptation, the convolution between the preirradiation leakage current distribution and the radiation-induced increase leakage current distribution presented in (1) is possible. In (4), μ can be expressed as

$$\mu = V_{\text{dep}} \times \gamma_{\text{dark}} \times \text{DDD} \quad (5)$$

where V_{dep} is the considered depleted volume in μm^3 and DDD is the DDD in $\text{TeV} \cdot \text{g}^{-1}$. The term γ_{dark} is assumed independent of temperature and annealing and is expressed as

$$\gamma_{\text{dark}} = \frac{K_{\text{dark}}}{\nu_{\text{dark}}} \quad (6)$$

where K_{dark} is the Srour factor defined in [13] and estimated at $K_{\text{dark}} = 0.098 \text{ e}^- \cdot \text{s}^{-1}/\text{TeV} \cdot \text{g}^{-1}/\mu\text{m}^3$ after four weeks annealing at $22 \text{ }^\circ\text{C}$ [13].

REFERENCES

- [1] E. R. Fossum and D. B. Hondongwa, "A review of the pinned photodiode for CCD and CMOS image sensors," *IEEE J. Electron Devices Soc.*, vol. 2, no. 3, pp. 33–43, May 2014.
- [2] S. Lauxtermann, A. Lee, J. P. Stevens, and A. Joshi, "Comparison of global shutter pixels for CMOS image sensors," in *Proc. IEEE Int. Image Sensor Workshop (IISW)*, Jun. 2007, p. 8. [Online]. Available: <http://www.imagesensors.org/Past%20Workshops/2007%20Workshop/Hyperlinked%20Contents.htm>
- [3] G. Meynants, "Global shutter imagers for industrial applications," *Proc. SPIE*, vol. 9141, May 2014, Art. no. 914108. [Online]. Available: <https://www.spiedigitallibrary.org/conference-proceedings-of-spie/9141/914108/Global-shutter-imagers-for-industrial-applications/10.1117/12.2060072.full?SSO=1>
- [4] V. Goiffon, "Radiation effects on CMOS active pixel image sensors," in *Ionizing Radiation Effects in Electronics: From Memories to Imagers*. Boca Raton, FL, USA: CRC Press, 2015, pp. 295–332.
- [5] C.-T. Sah, R. N. Noyce, and W. Shockley, "Carrier generation and recombination in P-N junctions and P-N junction characteristics," *Proc. IRE*, vol. 45, no. 9, pp. 1228–1243, Sep. 1957.
- [6] I. H. Hopkins and G. R. Hopkinson, "Random telegraph signals from proton-irradiated CCDs," *IEEE Trans. Nucl. Sci.*, vol. 40, no. 6, pp. 1567–1574, Dec. 1993.
- [7] G. R. Hopkinson, C. J. Dale, and P. W. Marshall, "Proton effects in charge-coupled devices," *IEEE Trans. Nucl. Sci.*, vol. 43, no. 2, pp. 614–627, Apr. 1996.
- [8] J. Bogaerts, B. Dierickx, and R. Mertens, "Random telegraph signals in a radiation-hardened CMOS active pixel sensor," *IEEE Trans. Nucl. Sci.*, vol. 49, no. 1, pp. 249–257, Feb. 2002.
- [9] A. Jay *et al.*, "Simulation of single particle displacement damage in silicon—Part II: Generation and long-time relaxation of damage structure," *IEEE Trans. Nucl. Sci.*, vol. 64, no. 1, pp. 141–148, Jan. 2017.
- [10] T.-H. Tsai, D. Marchesan, N. Faramarzpour, M. Sonder, and E. Fox, "Twinkling behavior in ultra-high-resolution CMOS global shutter pixels," in *Proc. IEEE Int. Image Sensor Workshop (IISW)*, Vaals, The Netherlands, Aug. 2015, pp. 98–101.
- [11] V. Goiffon, G. R. Hopkinson, P. Magnan, F. Bernard, G. Rolland, and O. Saint-Pe, "Multilevel RTS in proton irradiated CMOS image sensors manufactured in a deep submicron technology," *IEEE Trans. Nucl. Sci.*, vol. 56, no. 4, pp. 2132–2141, Aug. 2009.
- [12] C. Durnez, V. Goiffon, C. Virmontois, J.-M. Belloir, P. Magnan, and L. Rubaldo, "In-depth analysis on radiation induced multi-level dark current random telegraph signal in silicon solid state image sensors," *IEEE Trans. Nucl. Sci.*, vol. 64, no. 1, pp. 19–26, Jan. 2017.
- [13] J. R. Srour and D. H. Lo, "Universal damage factor for radiation-induced dark current in silicon devices," *IEEE Trans. Nucl. Sci.*, vol. 47, no. 6, pp. 2451–2459, Dec. 2000.
- [14] P. W. Marshall, C. J. Dale, and E. A. Burke, "Proton-induced displacement damage distributions and extremes in silicon microvolumes charge injection device," *IEEE Trans. Nucl. Sci.*, vol. 37, no. 6, pp. 1776–1783, Dec. 1990.
- [15] R. Germanicus *et al.*, "Evaluation and prediction of the degradation of a COTS CCD induced by displacement damage," *IEEE Trans. Nucl. Sci.*, vol. 49, no. 6, pp. 2830–2835, Dec. 2002.
- [16] O. Gilard, E. Martin, T. Nuns, C. Inguibert, and J.-P. David, "Statistical analysis of random telegraph signal maximum transition amplitudes in an irradiated CMOS image sensor," *IEEE Trans. Nucl. Sci.*, vol. 61, no. 2, pp. 939–947, Apr. 2014.
- [17] C. Inguibert *et al.*, "Modeling the dark current non-uniformity of image sensors with GEANT4," *IEEE Trans. Nucl. Sci.*, vol. 61, no. 6, pp. 3323–3330, Dec. 2014.
- [18] J.-M. Belloir *et al.*, "Pixel pitch and particle energy influence on the dark current distribution of neutron irradiated CMOS image sensors," *Opt. Express*, vol. 24, no. 4, pp. 4299–4315, Feb. 2016.
- [19] V. Goiffon, P. Magnan, O. Saint-Pé, F. Bernard, and G. Rolland, "Ionization versus displacement damage effects in proton irradiated CMOS sensors manufactured in deep submicron process," *Nucl. Instrum. Methods Phys. Res. A, Accel., Spectrometers, Detectors Assoc. Equip.*, vol. 610, no. 1, pp. 225–229, 2009.
- [20] J. R. Srour and R. A. Hartmann, "Enhanced displacement damage effectiveness in irradiated silicon devices," *IEEE Trans. Nucl. Sci.*, vol. 36, no. 6, pp. 1825–1830, Dec. 1989.
- [21] J. Bogaerts, B. Dierickx, and R. Mertens, "Enhanced dark current generation in proton-irradiated CMOS active pixel sensors," *IEEE Trans. Nucl. Sci.*, vol. 49, no. 3, pp. 1513–1521, Jun. 2002.
- [22] M. S. Robbins and L. G. Rojas, "An assessment of the bias dependence of displacement damage effects and annealing in silicon charge coupled devices," *IEEE Trans. Nucl. Sci.*, vol. 60, no. 6, pp. 4332–4340, Dec. 2013.
- [23] C. Virmontois *et al.*, "Total ionizing dose versus displacement damage dose induced dark current random telegraph signals in CMOS image sensors," *IEEE Trans. Nucl. Sci.*, vol. 58, no. 6, pp. 3085–3094, Dec. 2011.
- [24] C. Virmontois *et al.*, "Dark current random telegraph signals in solid-state image sensors," *IEEE Trans. Nucl. Sci.*, vol. 60, no. 6, pp. 4323–4331, Dec. 2013.
- [25] B. Pain, T. Cunningham, B. Hancock, C. Wrigley, and C. Sun, "Excess noise and dark current mechanisms in CMOS imagers," in *Proc. IEEE Workshop CCD's Adv. Image Sensors*, Nagano, Japan, 2005, pp. 145–148.
- [26] H. Yamashita, M. Maeda, S. Furuya, and T. Yagami, "Analysis of dark current in 4-transistor CMOS imager pixel with negative transfer-gate bias operation," in *Proc. IEEE Int. Image Sensor Workshop (IISW)*, Bergen, Norway, Jun. 2009, pp. 1–4.
- [27] P. A. Martin, B. G. Streetman, and K. Hess, "Electric field enhanced emission from non-Coulombic traps in semiconductors," *J. Appl. Phys.*, vol. 52, no. 12, pp. 7409–7415, 1981.
- [28] W. P. Noble, S. H. Voldman, and A. Bryant, "The effects of gate field on the leakage characteristics of heavily doped junctions," *IEEE Trans. Electron. Devices*, vol. 36, no. 4, pp. 720–726, Apr. 1989.
- [29] C. Y.-P. Chao *et al.*, "Random telegraph noises in CMOS image sensors caused by variable gate-induced sense node leakage due to X-ray irradiation," *IEEE J. Electron Devices Soc.*, to be published. doi: [10.1109/JEDS.2019.2893299](https://doi.org/10.1109/JEDS.2019.2893299). [Online]. Available: <https://ieeexplore.ieee.org/abstract/document/8612927>
- [30] B. R. Hancock and G. A. Soli, "Total dose testing of a CMOS charged particle spectrometer," *IEEE Trans. Nucl. Sci.*, vol. 44, no. 6, pp. 1957–1964, Dec. 1997.